Design and development of a 1 kW-class helicon antenna thruster

IEPC-2015-297/ISTS-2015-b-297

Presented at Joint Conference of 30th International Symposium on Space Technology and Science, 34th International Electric Propulsion Conference and 6th Nano-satellite Symposium
Hyogo-Kobe, Japan
July 4–10, 2015

Mario Merino,* Jaume Navarro,† Santiago Casado,‡ Eduardo Ahedo§
Equipo de Propulsión Espacial y Plasmas (EP2), Universidad Carlos III de Madrid, Leganés, Spain

Victor Gómez,¶ Mercedes Ruiz‖
SENER Ingeniería y Sistemas, Tres Cantos, Madrid, Spain
and
Eduard Bosch, José González del Amo
ESA ESTEC, Noordwijk aan Zee, The Netherlands

A Helicon Plasma Thruster prototype in the 0.5–1.5 kW range is being designed and built by EP2 and SENER. The prototype is proposed as a flexible testing platform for different geometries, magnetic configurations, antennas, frequencies and gases. The goal of the prototype is to verify the prediction of current models, understand the power loss mechanisms in the helicon plasma thruster, and investigate the optimization of its performance. The lessons learned from the first test campaign at ESA-ESTEC-EPL will help to improve the design and scale up to higher powers in the future. This paper presents the preliminary analysis and design results and discusses the main aspects that are expected to drive performance of the device.

I. Introduction

HELICON plasma sources are being used with great success to create high-density plasma sources for industrial applications.[1,2] In the last years, this type of technology has been proposed to create a novel type of space plasma thruster.[3,4,5,6] As it does not require a neutralizer or accelerating grids, the helicon plasma thruster (HPT) has good promise in terms of design simplicity, robustness, thrust density, and expected lifetime. Moreover, the use of a magnetic nozzle[7] (MN) to accelerate the plasma enables in-flight nozzle modification with an extended throttleability range. The HPT can also operate on different propellants and power levels.

These expected advantages have put the HPT in the spotlight of many research groups in the last years: a sizable number of prototypes have been built and tested (see, in particular, Refs. 4,8,9,10,11), and effort has been done to understand and model the physics of the device (Refs. 12,13,14,15,16,17). Notwithstanding, most laboratory prototypes still exhibit a low thrust efficiency below 5%, with some exceptions.[5] A brief review of some of these prototypes can be found in Ref. 18. These rather poor performance figures and the disagreement between different experiments could be caused by an insufficient propellant utilization, low electron temperatures, or inefficient confinement. In general, there is still an incomplete understanding of

*Assistant Professor, Aerospace Engineering department, mario.merino@uc3m.es.
†PhD Student.
‡MSc student.
§Professor, Aerospace Engineering department, eduardo.ahedo@uc3m.es.
¶System Engineer, Aerospace and Control Systems section, victor.gomez@sener.es.
‖Project Manager, Aerospace and Control Systems section, mercedes.ruiz@sener.es.

the internal and external plasma physics, the interaction of the RF waves with the plasma, and the power loss mechanisms.

Building on the first results and the theoretical framework in Ref. 16, and based on the conclusions of the ESA-funded project 'Helicon Plasma Thruster for Space Missions', EP2 and SENER are designing a new HPT prototype in the range 0.5-1.5 kW. The main goal of this development is to create a flexible test platform to aid in understanding the efficiency and utilization problems that affect these devices, test the limits of HPTs, and identify points for improvement for an optimal HPT design. The device is also being built with the objective to facilitate the escalation of HPTs to high power (10-20 kW) in the future. A first test campaign on this device is scheduled for the last quarter of 2015 at ESTEC (ESA) facilities, where the plasma properties and the propulsive figures of merit will be measured under different operating conditions and thruster configurations.

This paper presents the HPT prototype design, covering the RF generator, the antenna, the plasma-wave interaction process, the internal plasma dynamics, and the external MN expansion. Previous models for each of these parts have been connected together and used to provide the numerical estimate of the performance of the device. A sensitivity analysis has been carried out on the main problem parameters to set the design point of HPT-05.

The rest of the paper is structured as follows. Section II describes the prototype elements and its design point. Then, Section III briefly discusses the simulated performance of the device, and the key aspects of the HPT operation that are deemed to drive its performance. Section IV addresses the planned tests and measurements. Finally, conclusions and future work are listed in Section V.

II. HPT Prototype design overview

The high-level requirements of HPT-05 prototype are to create a simple, robust, and repeatable design in the 0.5–1.5 kW input power range. The first tests will run on argon at less than 70 sccm (2 mg/s). The design should constitute a flexible test platform, and allow exploring a wide range of the relevant control variables (chamber length L, mass flow $\dot{m}$, power P, magnetic field strength B, and RF frequency ω_{RF}). It should also be possible to carry out modifications of the design quickly and in a straightforward manner, as well as instrument it with diagnostics (thermocouples, probes, etc).

The main design degrees of freedom are the ionization chamber dimensions, the input mass flow, the RF power and frequency, the antenna shape and location, the magnetic field strength and geometry inside the chamber, and the shape of the external MN. All these variables interact with each other in a non-trivial way and affect all processes in the thruster, from ionization to internal plasma losses and external expansion. Therefore, its choice must come from a careful analysis of all these processes simultaneously. The nominal operation point of HPT-05 has been chosen according to the optimum performance observed in EP2 simulations of the plasma creation and expansion, and the most relevant values are gathered in Table 1.

Table 1. Summary of nominal values of the HPT-05 plasma thruster prototype.

Ionization chamber dimensions [cm]	Length: 15; Inner radius: 1.5
Mass flow [sccm]	50 (1.5 mg/s)
Power input at RF generator [W]	1000
Magnetic field in chamber [G]	400
Antenna RF frequency [MHz]	13.56
Antenna geometry [cm]	Half-helical, 7.5 cm long

A CAD overview of the assembled thruster is shown in Fig. 1. HPT-05 is composed of several elements:

- First, the main structure and positioning system for other elements, made of a circular mounting anodized aluminum backplate and a set of rods.
- Second, a cylindrical quartz tube inserted coaxially into the backplate serves as the HPT-05 ionization chamber.
- Third, a half-helical antenna surrounds the ionization chamber. The antenna feed is passed though the gap between the two solenoids, and the solenoid supports serve as a Faraday cage to limit the amount

of RF power radiated to free space.

- Fourth, a tunable RF generator (not shown) allows to generate and deliver the required RF power to the antenna. The RF generator is outside of the vacuum chamber during testing and connected to the HPT-05 via feed-throughs. It includes the necessary impedance matching circuitry.

- Fifth, the injector system is composed of the gas inlet tube and a diffusing injector. The whole unit can slide up and down the tube in a similar manner as in Ref. 10, allowing to change the effective chamber length.

- Sixth, two solenoids and a magnetic nozzle (MN) coil constitute the main magnetic generator. These elements are supported coaxially by the mounting rods. The electromagnets can be optionally water-cooled with an external jacket that allows to reach higher values of the magnetic field. The current through the MN and the solenoids are independently controllable. Also, the injector system is also provisioned with space for an annular permanent magnet that controls the plasma confinement at the rear wall of the ionization chamber.

In the following subsections, these components and the physical processes associated with them are discussed in more detail.

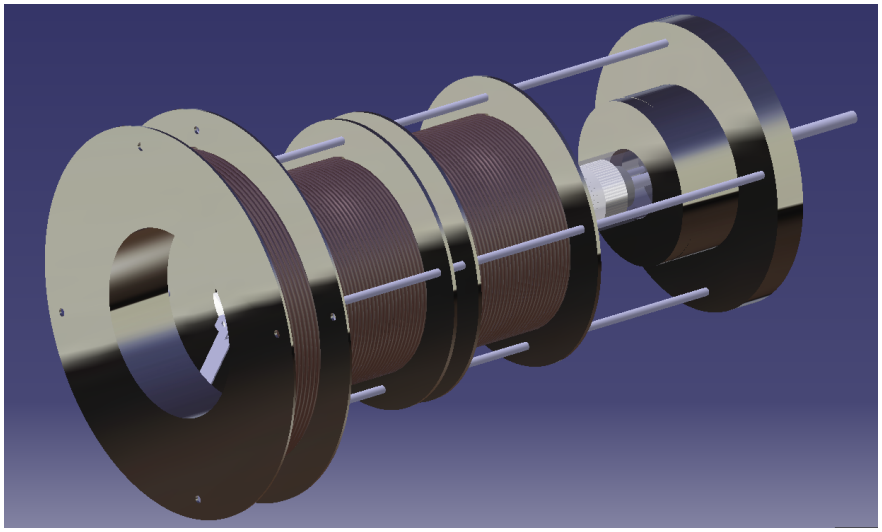

Figure 1. Overview of the assembled HPT-05 plasma thruster prototype.

A. Ionization chamber

The purpose of the ionization chamber is to hold the neutral gas in the ionization region long enough to allow its efficient ionization into a plasma. As explained in Refs. 15, 16, 17, when the RF wave energizes the electrons they have a chance of ionizing or exciting neutrals upon collisions. Excitation (and later de-excitation, or permanence as a meta-stable state) is a major loss mechanism at low electron temperatures, i.e. below 5–7 eV. Efficient ionization requires high electron temperatures (> 10 eV) and $\lambda_{ion} \ll L$, i.e., an ionization mean free path smaller than the chamber length. The chamber dimensions also must be adequate for the desirable electromagnetic wave modes to propagate in it.

The chamber material is exposed to the continuous heat flux caused by plasma contact and radiation. Ions and electrons reaching the wall deposit their energy on it and recombine. For this reason, a heat resistant, low thermal expansion material (quartz) is chosen for the ionization chamber tube. Plasma conduction to the walls is largely limited by the confining magnetic field that protects them. Good electron magnetization is required to maintain low plasma losses to the walls. In other words, we require $\ell_e \ll R$ (electron Larmor radius smaller than the tube radius) and $\chi_H \gg 1$ (Hall parameter larger than 1).

Using the model of Ref. 16 to estimate the performance of the chamber and the plasma-wave interaction model of Ref. 17, 19, we have sized simultaneously the nominal chamber dimensions, the mass flow rate

(which dictates the neutral density in the source) and the magnetic field. Simulations indicate that plasma transport and chamber efficiency is strongly influenced by the electron temperature T_e that can be achieved in the source. This is one of the main performance drivers of the HPT. Therefore, devising methods to obtain high T_e values is one of the highest priorities of this experimental work.

B. RF antenna

The helicon antenna is the interface to the plasma to deliver the RF power. When electric current circulates on the antenna and waves are emitted, they can be: (*i*) reflected by the plasma, (*ii*) enter the plasma domain, (*iii*) be radiated to free space, or (*iv*) be reabsorbed by the antenna itself (as reactive power). The free-space radiation can be limited by using a conducting Faraday cage around the device, which will cause the reflection of the wave back to it. The fraction of RF power that enters the plasma can in turn traverse it and leave it, or remain trapped in it. This last part of the RF power is eventually absorbed by the electrons.

The antenna design is a delicate part of the prototype, as its shape conditions the wave modes that will be excited in the plasma. The design geometry is currently being selected by searching for high plasma resistance and high power factor, which will facilitate the power matching with the power source. This search is done based on the plasma-wave interaction model that has been previously described in Refs. 20,21,17,19. Briefly stated, the model considers a cylindrical, fully-ionized plasma column of radius R, length L and density n_0, contained in a conducting cage of radius $r_w > R$. An axial magnetic field B_0 confines the plasma, and the antenna surrounds the plasma tube with radius r_a (where $r_w > r_a > R$) and length $2a$, as shown in Fig. 2. The plasma is modeled through the dielectric tensor for a cold plasma. The linearity of the Maxwell problem allows decomposing the electromagnetic fields in Fourier series in time, azimuthally and axially.[19] By also representing the antenna geometry as a Fourier expansion, the contribution of the different modes can be evaluated separately. The plasma impedance can be computed from the solution of the fields in Maxwell equations.[22,21,20]

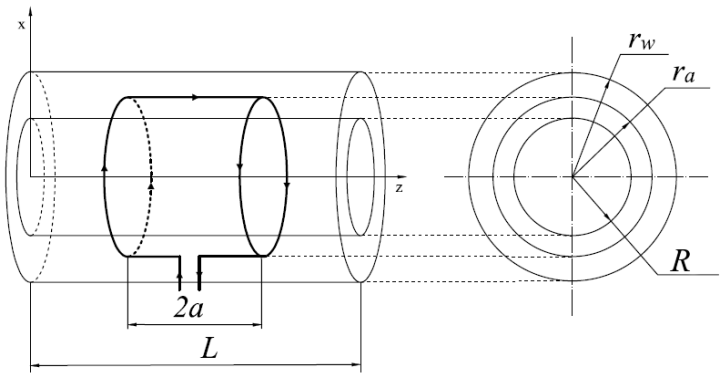

Figure 2. Sketch of the geometry for the wave-plasma interaction model.

After evaluating different antenna geometries and the obtained resistive power absorbed by the plasma, the two preliminary selected candidates are the *Nagoya III* and the *half-helical* type antennas. The plasma resistance under those geometries is shown in Fig. 3 for a uniform plasma density in the tube. Results show a similar performance between the Nagoya III and the half-helical antenna types, with a slightly better plasma resistance in the case of the half-helical antenna for a broad range of B_0 in the nominal case (depicted in continuous lines in Figure 3). In both cases, increasing RF frequency improves the resistance value. Tests will check these results and also explore higher frequencies. The half-helical antenna has been chosen for HPT-05. Further and more detailed investigation of the antenna and wave-plasma interaction problem can be found in Ref. 23.

It is interesting to evaluate the influence of the conductive boundary condition that has been imposed on the exit plane of the tube to close the model, and in particular, its effect on the calculated resistive power. The exact length of the conductive cage L and the magnetic field strength B_0 can change depending on the leading mode of the RF wave that fits in the cage. Small variations of either of these parameters cause a non-monotonic behavior of the plasma resistance, as it can be seen in Fig. 3. Figure 4 shows the variation of the plasma resistance as a function of the cage length L, for nominal operating conditions. In the long plasma

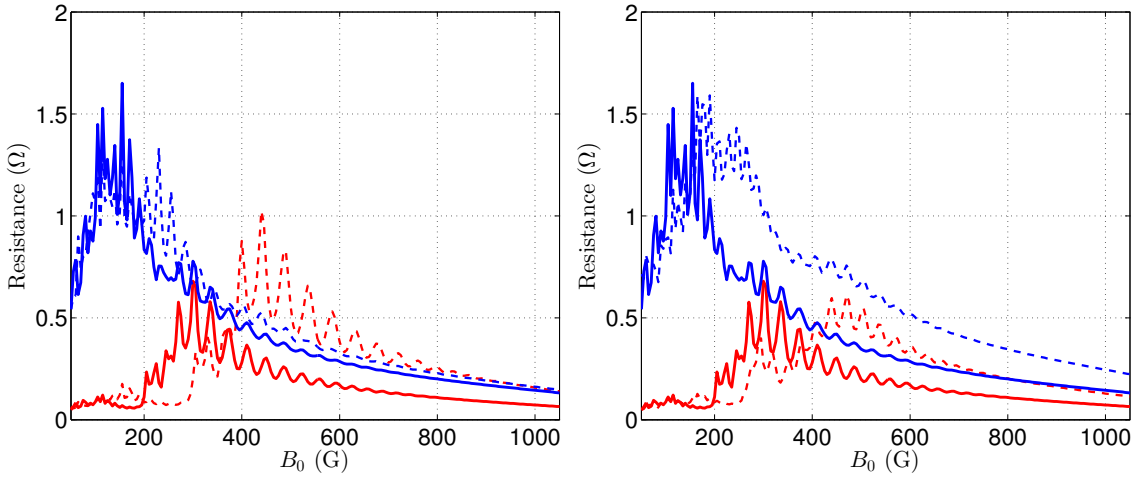

Figure 3. Performance evaluation of the Nagoya III and half-helical type antennas for different conditions. Blue lines represent the half-helical type antenna; red lines represent the Nagoya III type antenna. (left): Plasma resistance as a function of the nominal magnetic field B_0, for $\omega_{RF} = 13.56$ MHz, $\dot{m}_{Ar} = 1.5$ mg/s. Continuous lines represent the nominal plasma tube length with $L/R = 10$; dashed lines represent $L/R = 15$. (right): Plasma resistance as a function of the nominal magnetic field B_0, for the case of $\omega = 13.56$ MHz, $L/R = 10$. Continuous lines represent the nominal argon mass flow rate of $\dot{m}_{Ar} = 1.5$ mg/s; dashed lines represent $\dot{m}_{Ar} = 2.5$ mg/s.

tube limit, the influence of the downstream conducting wall becomes negligible, and oscillations disappear (like for high B_0 values).

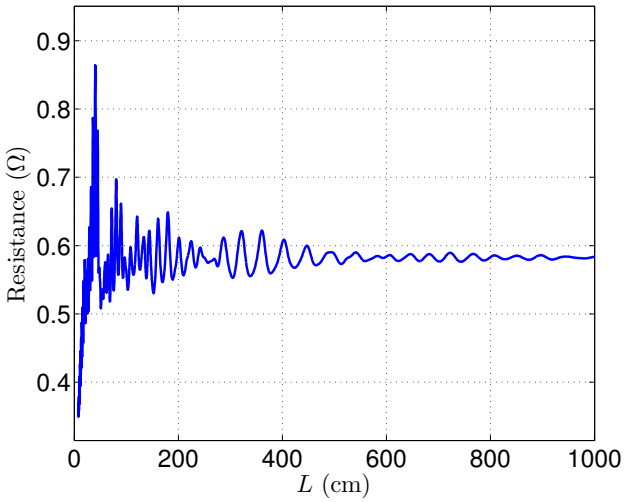

Figure 4. Plasma resistance as a function of the plasma tube length L, for $\omega = 13.56$ MHz, $\dot{m}_{Ar} = 1.5$ mg/s, $R = 1.5$ cm, $B_0 = 400$ G.

Physically, two designs are being considered at this stage for the half-helical antenna. On the one hand, a design based on twisted copper wires to reduce the antenna losses due to the skin effect is considered. This design has a drawback regarding the antenna stiffness, requiring some Teflon rings to conform the half-helical shape. On the other hand, a design based on a blended copper strip is considered, similar to that considered in Ref. 24, which has higher losses due to the skin effect but is stiff. The preliminary thermal analysis results indicate the latest design would be more suitable to withstand the temperatures that could be reached in the antenna.

C. RF power generator and impedance matching

The RF power generator and impedance matching unit is an important element of HPT-05. It generates the RF wave that creates the plasma and must ensure the optimal power transmission to the plasma according to its impedance. The capability to generate RF power and transmit it in an efficient manner is taken into account in the overall thrust efficiency η figure of Section III, which includes the RF generation efficiency η_{RF} as one of the contributing factors.

In order to get the most flexible performance, SENER is developing a Radio-Frequency Generator and Processing Unit (RFGPU) which is able to provide a wide range of operational values to find the best parameters for the HPT during the testing activities. The RFGPU allows power adjustment up to 1kW DC input for several discrete frequencies in the range of 5–30 MHz. Moreover, it provides impedance matching capabilities to the system, maximizing the equipment power transmission efficiency at each operational point and, therefore, the thruster efficiency.

The RFGPU consists of different blocks assembled together including a local oscillator, where the RF wave is generated, an exciter, which amplifies the signal before a power amplifier stage, working as a class E amplifier, and a matching network adapting the variable plasma impedance to that of the RF system. The schematic of these components is shown in the block diagram of Fig. 5.

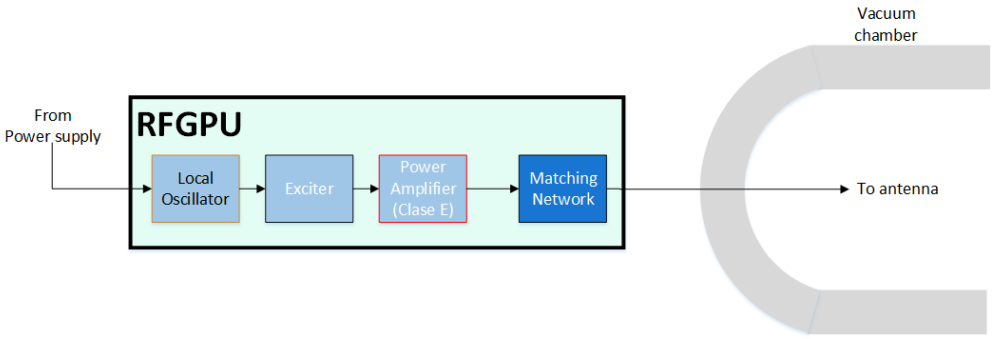

Figure 5. RFGPU block diagram.

The efficiency of the RFGPU is expected to be above $\eta_{RF} = 75\%$ in all the operational envelope, taking into account all the power losses along the different blocks, wires and feedthroughs involved in the antenna feeding circuit. Optimal power transmission efficiency is sacrificed against operational flexibility in the present design. Maximum efficiency could be reached for a specific pair of power and frequency values up to 90% of input DC power. Next development stages will allow higher efficiencies once the optimum HPT working point will be set, with values around $\eta_{RF} = 95\%$ efficiency.

D. Neutral gas injector and propellant management

The HPT neutral gas injector has been designed to fit into the internal diameter of the plasma chamber. It shall withstand the heat fluxes generated by the plasma, avoiding thermal conduction to the elements placed upstream of it. This is achieved using a material with low conductivity. The design with the diffuser allows the gas to be injected homogeneously at all radii through multiple perforations. Additionally, the present design aims to increase the residence time of neutrals in the tube and thus the likelihood of ionization collisions (which would lead to a higher utilization factor).

The injector is attached to the end of the gas feed. The whole set-up can be displaced up and down to adjust the axial position of the element, allowing a variable chamber length. As structural element, the injector also hosts the permanent magnet of the magnetic field circuit.

The propellant management is performed using Bronkhorst® digital pressure controllers. These controllers, situated outside the vacuum chamber, are connected to the propellant tank on one side and to the vacuum chamber feedthrough on the other. The controller model considered for the experiments is the P-602CV, which can provide mass flow control capability within the range 0.5–2 mg/s Ar considered in the design.

E. Magnetic field circuit

The magnetic field generator is the last key component of a HPT. It can be made of permanent magnets, electromagnets, or a combination thereof. The $\boldsymbol{B}$ field has the important tasks of (*i*) allowing the wave propagation in the plasma, (*ii*) reducing plasma losses to the internal thruster walls, and (*iii*) creating the external MN for the supersonic plasma expansion.

An electromagnet setup is chosen for the prototype to allow varying the intensity and shape of the magnetic field in the tests. The design and optimization of the electromagnet part of the generator is carried out following the algorithm and model of Ref. 22: the solenoids and coils are discretized as point current loops, for which the analytical magnetic field solution is direct. Then, the magnetic performance or cost function f is defined, which allows to compare different configurations. This cost function states that, for a given field geometry, the product $M_{mag}P_{mag}$ (mass and power of the magnetic generator) depends only on the scale of the device, the field strength, the resistivity of the material, and the density of the material. In particular, it scales as:

$$M_{mag}P_{mag} \propto R^4 B_0^2. \tag{1}$$

Several coil layouts were analyzed that produce desirable geometries: smooth magnetic field inside the chamber, and long, slowly-divergent MN outside of it. A configuration with low magnetic cost was chosen, which is displayed in Fig. 6. It is composed of two solenoids that surround the ionization chamber. The solenoid separation can be changed to cover longer tubes. A MN coil, with a larger radius, is also present. The electric current through this coil is independently controlled from that through the solenoids, to allow increasing/decreasing the MN throat area and strength. The inner radius of the solenoids is fixed at twice the inner radius of the ionization chamber, to leave a gap large enough for the antenna, and limit its RF interaction with them. In the rear part of the ionization chamber, the optional permanent rare-Earth magnet creates a magnetic cusp that can further reduce plasma losses there. This second magnetic configuration (modeling the permanent magnet as two additional current loops) is also shown in Fig. 6.

To maximize the flexibility of the prototype, electromagnets are intentionally larger than strictly required. Each solenoid is allocated 3 kg of copper, and 2.2 kg are allocated to the MN coil. At 400 G, each solenoid carries 3000 ampere-turns and the nozzle 1500 ampere-turns. To validate the results of this simple model, they were compared against FEM simulations of the magnetic field. The value of the power consumed by each coil was calculated with the copper resistance and the current values, obtaining differences below 1% with respect to the analytical design model.

The employed copper wires are supported by an anodized aluminum frame that is mounted on the HPT structure. They have a polyurethane insulating coating layer that can withstand up to 200 °C, which limits the power consumption of the elements. To ensure that high values of the magnetic field can be safely reached, a water-cooling system is optionally included in each coil. Control of the magnetic field strength achieved with the proposed magnetic topology is attained by varying the current through each element. The axial position of the components can be adjusted to provide additional flexibility and control of the field distribution inside the chamber in a similar manner to Ref. 10.

Regarding the permanent magnet at the rear wall, a neodymium ring permanent magnet of grade is N35UH has been selected. Neodymium presents better properties than Samarium-Cobalt magnets for the present application, reaching higher fields and magnetic energy products.

Lastly, the external MN is the accelerating stage of HPT-05. The hot electrons expand outward under the radial confinement of the magnetic field, creating an axial ambipolar electric field that accelerates ions. In this way, internal energy is converted into directed kinetic energy.[7] The magnetic force on electron azimuthal currents creates a reaction on the thruster, which gives rise to the magnetic thrust force. Finally, downstream plume formation requires adequate separation from the closed magnetic lines (plasma detachment[25,26]). By increasing the relative intensity through the MN coil, it is possible to reduce the magnetic throat area and increase the MN strength. This has a direct influence on the mass flow rate of ions that can be extracted from the source and the area expansion ratio. Investigation of this phenomenon is planned for the first experimental test campaigns.

III. Preliminary performance analysis

This section summarizes the different processes that define the propulsive performances of HPT-05, and presents a preliminary estimation of these figures at its nominal operating point of Table 1. To compute

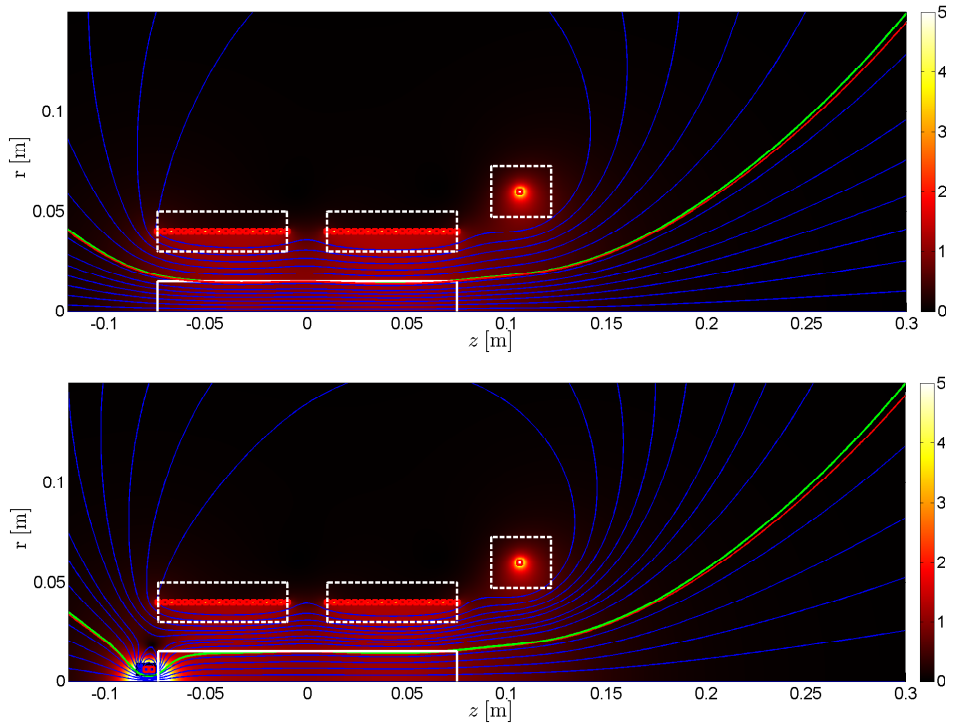

Figure 6. Chosen magnetic field generator without (up) and with (down) the optional permanent magnet. All elements are modeled analytically as equivalent punctual current loops. The green line defines the magnetic line that passes by the exit border of the ionization chamber. Additional magnetic lines are shown in blue. The background color is the magnetic field intensity, B/B_0, with B_0 evaluated at the origin of coordinates.

the thrust efficiency of the device we need to follow the power from the moment it enters the RFGPU to the formation and expansion of the plasma beam. Several partial efficiencies are defined to facilitate the discussion of the different processes involved:

1. Of the total input power P_{in} that enters RFGPU, only $P_{RF} = \eta_{RF} P_{in}$ is converted to RF power at the antenna. The efficiency η_{RF} includes the RFGPU, transmission line and ohmic antenna losses.

2. Part of this RF power is absorbed by other materials than the plasma, or lost to free space.In general, the absorption efficiency η_{abs} is defined, as the ratio between the power absorbed by the electrons, P_{abs}, and P_{RF}: $P_{abs} = \eta_{abs} P_{RF}$. Free space losses, however, do not occur in a closed vacuum chamber. Hence for the laboratory tests, it can be assumed $\eta_{abs} = 100\%$.

3. The power absorbed by the electrons P_{abs} can be invested into ionizing the neutral gas, exciting undesired energy states (where energy later decays as photon radiation or remains bounded to the atom in a meta-stable form), or remain in the electron population increasing its internal energy: $P_{abs} = P_{ion} + P_{exc} + P_e$:

   (a) P_{ion} is readily calculated from the mass flow rate $\dot{m}$ once the propellant utilization factor η_u is known (ratio of ion mass flow at the exit to neutral mass flow at the inlet), and from the plasma flux to the walls $\dot{m}_{wall}$:

   $$P_{ion} = (\eta_u \dot{m} + \dot{m}_{wall}) \frac{E_{ion}}{m_i} \tag{2}$$

   where E_{ion} is the ionization energy. Ionization power of $\eta_u \dot{m}$ are necessary losses for the operation of the HPT (i.e., this energy remains frozen in the plasma beam). The rest of ionization losses are unnecessary, and are associated to plasma losses to the walls, where ions recombine releasing that energy. Thus, reducing $\dot{m}_{wall}$ with successful magnetic confinement is a crucial aspect in an efficient HPT.

(b) We can estimate P_{exc} to be proportional to P_{ion} (i.e., only a fraction of the inelastic electron-neutral collisions successfully cause an ionization event): $P_{exc} = \alpha_{exc} P_{ion}$. As stated before, excitation losses depend strongly on the temperature of the electron population, T_e, with larger temperatures reducing the coefficient α_{exc}. Double ionization, etc can also be included in this power contribution. Most of P_{exc} is lost in radiation, which may heat up the chamber walls or (since they can be transparent at the relevant wavelengths) reach the surrounding HPT-05 elements.

(c) Note that a part of P_e also ends up lost to the lateral and back walls with $\dot{m}_{wall}$.

4. The other part of P_e can be converted into ion kinetic energy thanks to the ambipolar electric field. The fraction of P_{abs} that actually leaves the chamber with the plasma beam in the form of ion kinetic energy, electron internal enery, or heat fluxes, is denoted $P_{beam} = \eta_{cham} P_{abs}$.

5. Neglecting ionization and collisions outside of the source, P_{beam} is gradually converted into ion kinetic energy, accelerating the plasma jet and generating thrust. The obtained thrust depends strongly on the ion mass flow and the square root of the electron temperature. The small thrust contribution from unionized propellant leaving the source is ignored. Nonetheless, it is too optimistic to assume that complete expansion will be successfully achieved within the MN, before the applied magnetic field becomes too weak to guide the plasma. To reflect this, the expansion efficiency, η_{exp}, serves to limit the fraction of completed expansion. Also, the expansion is not 1D but incurs into 2D divergence losses as the jet opens. These losses are represented by the efficiency η_{div}. Successful plasma detachment is crucial to keep this efficiency high. The useful propulsive power is finally written as $P_{prop} = \eta_{div}\eta_{exp} P_{beam}$, and the resulting thrust force can be expressed as $F^2 = 2\dot{m}\eta_u P_{prop}$.

In summary, we may write the thrust efficiency of HPT-05 as:

$$\eta = \frac{F^2}{2\dot{m}P_{in}} = \eta_u \eta_{div} \eta_{exp} \eta_{cham} \eta_{abs} \eta_{RF}, \tag{3}$$

and the specific impulse is given by $I_{sp} g_0 = \sqrt{2P_{in}\eta/\dot{m}}$.

In the former, we have identified three key performance drivers of the HPT, leaving aside the RF wave generator: First, a high electron temperature is needed to ionize efficiently and obtain high thrust and I_{sp}. Reaching high temperatures is a priority in the present work, and experimental effort will be put into understanding the electron energization and power loss mechanisms that govern this important figure. Second, high confinement is required to minimize wall losses. Confinement is affected by magnetic strength, collisions, and anomalous diffusion (if any). Third, a smooth expansion in the MN that manages to complete the expansion with low divergence losses is crucial. The expansion is governed by the magnetic strength and the magnetic geometry.

To conclude, an estimation of the various partial efficiencies defined above in the case of HPT-05 can be done with the use of the models mentioned in previous sections.

- The RF efficiency η_{RF} is about 75% to maintain high flexibility; absorption, in the case of a laboratory experiment without free-space losses, approaches $\eta_{abs} = 100\%$.
- Chamber efficiency differs largely depending on the electron temperature and magnetic field strength: for $B_0 = 400$ G, models show it can be as low as $\eta_{cham} = 35\%$ at T_e =5–7 eV, or increase beyond $\eta_{cham} = 65\%$ at $T_e = 15$ eV and larger. As stated above, uncertainties (in anomalous diffusion, for instance) make it difficult to estimate a reliable value of T_e a priori.
- Utilization can be low at low temperatures ($< 60\%$ at 5–7 eV), but raises rapidly to near 100% beyond $T_e = 12$ eV. Again, the computation of this number is affected by the uncertainties in anomalous diffusion and other effects.
- The MN efficiencies η_{exp} and η_{div} can be computed quite accurately with the DIMAGNO code;[7] values around $\eta_{exp} = 80\%$ and $\eta_{div} = 75\%$ are expected for the present MN shape and average strength.

According to this preliminary estimation and within the validity of the assumptions taken, thrust efficiencies in the range $\eta = 10\%$–30% could be expected with the present prototype depending on the value of T_e achieved. Evidently, testing is necessary to validate this first estimate of the performance and devise further improvements.

A. Thermal response

At the same time that losses reduce efficiency, they mean a larger fraction of power delivered to the walls and other elements of the prototype, which may constitute a thermal problem.

Likewise, there exist ohmic losses in the antenna and in the magnetic generator circuit, which can raise the local temperature. Additionally, certain amount of radiation is received from the walls of the vacuum chamber, which are near room temperatuer. In steady state operation, the device radiates all the generated heat to the environment. The computation of the thermal response of HPT-05 is a complex problem that has to be analyzed to validate the proposed design.

1. Heat load model

The plasma heat loads are obtained from model simulation results as two contributions: one from plasma flux on the lateral and rear tube walls, and the other in the form of radiated energy by the plasma volume. At the design point, approximately, 126 W arrive the chamber walls due to the plasma flux to them, and an additional 83.4 W are radiated by the plasma excitation and de-excitation processes when $T_e = 15$ eV and $B_0 = 400G$ and under the assumptions of the model. Larger thermal loads may be expected, for instance, at lower magnetic fields.

The heat generation in the coils and the antenna is based on Ampere's law and depends on the power consumption, given by the current through each element and the resistance, which varies with the constituting material and the temperature. For the considered thermal model the resistance variation with the temperature is not considered to simplify the calculations.

2. Thermal control design

As mentioned in the magnetic generator circuit description, the limit operational temperature of each coil is determined by the copper insulating coating layer that can withstands only up to 200°C. To get acceptable temperatures at these elements at high magnetic field operation, a thermal control system is installed, which consists of a water cooling line embracing each coil. The temperature control of each element is reached by the combination of the tube section selection (design) and the water mass flow. This set up, while not optimal for space application, allows to create a very flexible HPT testing platform.

3. Thermal analysis

Thermal analyses are being performed based on worst case simulation. In addition to the modeled heat fluxes, the component geometries and their material thermal properties are included in the HPT thermal model. For the simulation, this model considers thermal radiation in vacuum and heat conduction to contiguous thermal nodes. The simulation includes detailed view factor calculations, operational margin estimations based on the maximum limit temperature of each element, and mean temperature estimation of all parts. The results of the thermal analysis will be used to assess the implemented design.

IV. HPT-05 initial test plan

As part of the program to characterize the ESA-ESTEC-EPL test facilities for the use of innovative thrusters, the HPT-05 prototype will be tested for several weeks in the last quarter of 2015 in the Corona vacuum chamber. This chamber has a pumping speed of 70,000 l/s Ar, which allows operating the device at high mass flow rates. The EPL laboratory is equipped with an ample number of high-quality plasma diagnostic systems that will be used to characterize the device. These tests constitute the first test campaign of this prototype, and have various objectives, some of which have already been indicated in previous sections.

Before the beginning of these tests, an extensive integrity check of the system will be carried out at EP2 and SENER premises, and the magnetic field with and without the rear permanent magnet will be characterized using B-probes.

First and foremost, the tests aim at demonstrating the nominal operation of the device. Power, plasma impedance, and thrust will be measured. Comparison against the predicted efficiency, thrust and specific impulse will allow to validate our EP2 models, identify and troubleshoot possible problems and shortcomings, and define future improvement steps.

Second, HPT-05 will be tested at varying values of the applied magnetic field, input power, Ar mass flow and chamber length to characterize the operational envelope and identify optimal operating points and obtain a first measurement of its throttleability.

Third, the device will be instrumented with thermocouples to validate the thermal model and measure the temperatures at steady state operation. Operation with and without the water cooling system will be considered.

Fourth, plasma measurements will be carried out at the exit plane of the ionization chamber and at several locations downstream along the axis and off-axis to characterize the plume expansion. A combination of a Faraday cups, Langmuir probes, and emissive probes will be used to resolve the plasma density, ambipolar potential, electron temperature and ion current in the plume. These measurements are essential to understand the operating regime of HPT-05, and will allow to validate the MN expansion model and study the phenomenon of plasma detachment. The integration of the plasma momentum at different sections will serve as an additional estimation of the thrust force and to identify the pressure and magnetic thrust contributions.[16,26]

After this test campaign, further investigation of HPT-05 will be carried out in the new testing facilites of EP2, at Universidad Carlos III de Madrid.

V. Conclusions

The design of the HPT-05 helicon plasma thruster prototype by EP2 and SENER has been presented and the major highlights discussed. The various components, their purpose, as well as the design process that has led to their sizing, have been described.

The choice of the nominal point of HPT-05 is based on the analysis of the performance of the prototype and its partial efficiencies, computed with the previously existing models and codes in EP2. The stress is put into developing a flexible test platform that enables us to explore the efficient operation regimes, validate our present understanding of the physical processes in the HPT, and advance the state of the art in this technology.

The expected performance values of the prototype have been presented. The HPT-05 is not yet optimized for efficiency, but verification of the computed estimations would mean a step forward with respect to existing prototypes. The thermal problem has been given particular attention.

Lastly, the objectives of the first test campaign at ESA-ESTEC-EPL facilities have been briefly commented on. These tests are scheduled for the last quarter of 2015. Further experimentation and improvement of the prototype will continue after this campaign in the new test facilities of EP2.

Acknowledgments

The authors would like to thank Flemming H. Pedersen for designs and contributions to the RF power generator and impedance matching system. EP2 group support has been provided by the Spanish R&D National Plan, grant number ESP2013-41052-P.

References

[1]Boswell, R., "Plasma production using a standing helicon wave," *Physics Letters A*, Vol. 33, No. 7, 1970, pp. 457–458.

[2]Chen, F., "Industrial applications of low-temperature plasma physics," *Physics of Plasmas*, Vol. 2, No. 6, 1995, pp. 2164.

[3]Gilland, J. and Hershkowitz, N., "Application of a helicon discharge to electric propulsion," *34th AIAA Joint Propulsion Conference*, Vol. 3934, 1998.

[4]Charles, C. and Boswell, R., "Current-free double-layer formation in a high-density helicon discharge," *Applied Physics Letters*, Vol. 82, 2003, pp. 1356.

[5]Batishchev, O., Sinenian, N., Celik, M., and Martinez-Sanchez, M., "Results from the mini-helicon thruster experiment," *APS Meeting Abstracts*, Vol. 1, 2007, p. 5005.

[6]Pavarin, D., Ferri, F., Manente, M., Curreli, D., Guclu, Y., Melazzi, D., Rondini, D., Suman, S., Carlsson, J., Bramanti, C., Ahedo, E., Lancellotti, V., Katsonis, K., and Markelov, G., "Design of 50W Helicon Plasma Thruster," *31th International Electric Propulsion Conference*, IEPC 2009-205, 2009.

[7]Ahedo, E. and Merino, M., "Two-dimensional supersonic plasma acceleration in a magnetic nozzle," *Physics of Plasmas*, Vol. 17, 2010, pp. 073501.

[8]Ziemba, T., Euripides, P., Slough, J., Winglee, R., Giersch, L., Carscadden, J., Schnackenberg, T., and Isley, S., "Plasma characteristics of a high power helicon discharge," *Plasma Sources Science and Technology*, Vol. 15, 2006, pp. 517.

[9]Batishchev, O., "Minihelicon Plasma Thruster," *IEEE Transaction on Plasma Science*, Vol. 37, 2009, pp. 1563–1571.

[10]Little, J. M. and Choueiri, E. Y., "Plasma transport in a converging magnetic field with applications to helicon plasma thrusters," *33th International Electric Propulsion Conference*, No. IEPC-2013-125, 2013.

[11]Trezzolani, F., Fabris, A. L., Pavarin, D., Selmo, A., and Manente, M., "Low Power Radio-Frequency Plasma Thruster Development and Testing," *33th International Electric Propulsion Conference*, No. IEPC-2013-153, 2013.

[12]Cho, S. and Lieberman, M., "Self-consistent discharge characteristics of collisional helicon plasmas," *Physics of Plasmas*, Vol. 10, 2003, pp. 882–890.

[13]Fruchtman, A., Makrinich, G., and Ashkenazy, J., "Two-dimensional equilibrium of a low temperature magnetized plasma," *Plasma Sources Science and Technology*, Vol. 14, 2005, pp. 152–167.

[14]Fruchtman, A., "Neutral depletion in a collisionless plasma," *Plasma Science, IEEE Transactions on*, Vol. 36, No. 2, 2008, pp. 403–413.

[15]Ahedo, E., "Parametric analysis of a magnetized cylindrical plasma," *Physics of Plasmas*, Vol. 16, 2009, pp. 113503.

[16]Ahedo, E. and Navarro, J., "Helicon thruster plasma modeling: Two-dimensional fluid-dynamics and propulsive performances," *Physics of Plasmas*, Vol. 20, 2013, pp. 043512.

[17]Martínez, D. and Ahedo, E., "Plasma-wave interaction in a helicon thruster," *32th International Electric Propulsion Conference*, No. IEPC-2011-047, 2011.

[18]Navarro, J., Ahedo, E., Merino, M., Urdampilleta, I., Ruiz, M., and del Amo, J. G., "Assessment of helicon plasma thruster technology for space missions," *Space Propulsion Conference 2014*, European Space Agency, 2014.

[19]Tian, B., Ahedo, E., and Navarro-Cavallé, J., "Investigation of Plasma-wave Interaction in Helicon Antenna Thrusters," *50th AIAA/ASME/SAE/ASEE Joint Propulsion Conference & Exhibit*, 2014.

[20]Shamrai, K. and Taranov, V., "Resonance wave discharge and collisional energy absorption in helicon plasma source," *Plasma Physics and Controlled Fusion*, Vol. 36, 1994, pp. 1719–1735.

[21]Cho, S., "The field and power absorption profiles in helicon plasma resonators," *Physics of Plasmas*, Vol. 3, 1996, pp. 4268.

[22]Navarro, J., Merino, M., Ahedo, E., Ruiz, M., and Sánchez, V., "Design of Helicon Plasma Thruster subsystems," 50^{th} *AIAA/ASME/SAE/ASEE Joint Propulsion Conference & Exhibit*, No. AIAA-2014-3699, AIAA, Washington DC, 2014.

[23]Tian, B., Ahedo, E., and Navarro-Cavallé, J., "Analysis of Antenna-Plasma Impedance in Helicon Antenna Thrusters," *34th International Electric Propulsion Conference*, No. 2015-b/IEPC-326, 2015.

[24]Carter, M., Baity Jr, F., Barber, G., Goulding, R., Mori, Y., Sparks, D., White, K., Jaeger, E., Chang-Diaz, F., and Squire, J., "Comparing experiments with modeling for light ion helicon plasma sources," *Physics of Plasmas*, Vol. 9, 2002, pp. 5097.

[25]Ahedo, E. and Merino, M., "On plasma detachment in propulsive magnetic nozzles," *Physics of Plasmas*, Vol. 18, 2011, pp. 053504.

[26]Merino, M. and Ahedo, E., "Plasma detachment in a propulsive magnetic nozzle via ion demagnetization," *Plasma Sources Science and Technology*, Vol. 23, 2014, pp. 032001.